Applied Catalysis B: Environmental 89 (2009) 635–644

Contents lists available at ScienceDirect

Applied Catalysis B: Environmental

journal homepage: www.elsevier.com/locate/apcatb

Synergistic effect of TiO_2 and iron oxide supported on fluorocarbon films. Part 1: Effect of preparation parameters on photocatalytic degradation of organic pollutant at neutral pH

F. Mazille, T. Schoettl, C. Pulgarin *

Institute of Chemical Sciences and Engineering, SB, GGEC, Ecole Polytechnique Fédérale de Lausanne, 1015 Lausanne, Switzerland

ARTICLE INFO

Article history:
Received 28 July 2008
Received in revised form 27 January 2009
Accepted 31 January 2009
Available online 6 February 2009

Keywords:
Heterogeneous photo-Fenton
TiO_2 photocatalysis
Polymer surface modification
Synergistic effects
Solar detoxification

ABSTRACT

Iron oxide and TiO_2 were immobilized on modified polyvinyl fluoride films in a sequential process. Synergic effects of iron oxide and TiO_2 on the polymer film were observed during the heterogeneous degradation of hydroquinone (HQ) in the presence of H_2O_2 at pH close to neutrality and under simulated solar irradiation. Within the degradation period, little iron leaching (<0.5 mg/L) was observed.

The surface of commercial polyvinyl fluoride (PVF) film was modified by TiO_2 under light inducing oxygen group (C–OH, C═O, COOH) formation on the film surface. During this treatment, TiO_2 nanoparticles simultaneously bind to the film, leading to PVF^f–TiO_2. The possible mechanistic pathway for the TiO_2 deposition and the nature of the polymer–TiO_2 interaction are discussed. Furthermore PVF and PVF^f–TiO_2 were immersed in an aqueous solution for the deposition of iron oxide layer by hydrolysis of $FeCl_3$, leading to PVF–Fe oxide and to PVF^f–TiO_2–Fe oxide respectively.

HQ degradation and mineralization mediated by PVF^f–TiO_2, PVF–Fe oxide and PVF^f–TiO_2–Fe oxide were investigated under different conditions. Remarkable synergistic effects were observed for PVF^f–TiO_2–Fe oxide possibly due to Fe(II) regeneration, accelerated by electron transfer from TiO_2 to the iron oxide under light.

1. Introduction

The degradation of organic anthropogenic substances has become an important issue during the last decades due to their increasing production. These compounds are bio-recalcitrant and not degraded by microorganisms during wastewater treatment. Because of the toxic, carcinogenic or endocrinal potential of many of them, their abatement is crucial to avoid accumulation in the environment damaging living species.

The application of advanced oxidation processes (AOPs) is an attractive alternative for the removal of bio-recalcitrant pollutants [1]. These degradation techniques are based on the generation of reactive oxygen species like hydroxyl ($OH^•$) and hydroperoxyl ($HO_2^•$) radicals. Among AOPs, photo-assisted processes use natural solar light as energy source. Their application in water and air purification [2,3], or disinfection [4], as well as in synthetic organic chemistry [5] have been reported. Among photo-assisted AOPs, TiO_2 photocatalysis and photo-Fenton oxidation are efficient routes for the degradation of recalcitrant compounds in water [6].

However these photocatalytic processes suffer from several practical limitations preventing wider application: (i) after treatment, separation of photocatalyst (highly dispersed TiO_2 nanoparticles or dissolved iron ions) is required; (ii) in the case of TiO_2 photocatalysis, light absorption by TiO_2 comprising only 4–6% of the solar spectrum limits the efficiency of this process; (iii) homogeneous photo-Fenton needs a pH ∼ 3 in order to prevent the formation of insoluble amorphous ferric oxy-hydroxides [7].

To overcome limitation (i), some studies have described the immobilization of TiO_2 on supports [8–10] including polymer films [11]. However, the activity of immobilized photocatalysts is generally low compared to suspensions. To make TiO_2 an efficient photocatalyst under visible light, doping with different species like iron [12], carbon [13], nitrogen–sulfur [14] among many others, has been reported. Immobilizing iron species like aqua-complexes or oxides on different supports [15–20] including polymer films [21] resulted in efficient photo-Fenton catalysts at pH close to 3. Nevertheless in the presence of ligands (aliphatic acids, humic acids, etc.) iron ions are likely to be released into the solution [22]. To overcome the slow kinetics when using either TiO_2 or Fenton mediated processes, the combination of iron oxide with TiO_2 is an attractive option since synergistic effects are likely to occur. Some recent studies described Fe_2O_3–TiO_2 coatings on glass [23] and activated carbon fiber [24]. Synergistic effects refer to the

* Corresponding author. Tel.: +41 21 693 47 20; fax: +41 21 693 61 61.
E-mail address: cesar.pulgarin@epfl.ch (C. Pulgarin).
URL: http://ggec.epfl.ch/page13443.html

0926-3373/$ – see front matter © 2009 Elsevier B.V. All rights reserved.
doi:10.1016/j.apcatb.2009.01.027

phenomena when the degradation rate of combined system is greater than the sum of its parts. These non-additive effects have recently been observed for the combination of suspended TiO_2 mediated photocatalysis with high frequency ultrasound [25], with ozonization [26] and when combining supported TiO_2 with homogeneous photo-Fenton oxidation [27].

This study presents a method to bind TiO_2 and iron oxide on Tedlar® polyvinyl fluoride (PVF) film. The PVF film has been selected due to its transparency, low cost (compared to DuPont Nafion®), high resistance to weathering, durability, mechanical resistance, chemical inertness, and absence of aging properties due to absence of plasticizers. The method to bind TiO_2 and iron oxide on PVF employs solar light, low temperature, needs short preparation time in aqueous solution, and generates C=O, C–OH, COOH groups on the PVF surface by TiO_2 photocatalysis as described by Kim et al. [28,29]. The produced photocatalysts (PVF^f–TiO_2, PVF–Fe oxide and PVF^f–TiO_2–Fe oxide) were characterized by scanning electron microcopy (SEM), X-ray photoelectron spectroscopy (XPS) and UV–vis spectroscopy.

The objective of this study is to report the performance of PVF^f–TiO_2–Fe oxide toward the degradation and mineralization of hydroquinone (HQ), a model compound representative for industrial pollutants.

2. Experimental

2.1. Chemicals

Hydroquinone, NaOH, HNO_3, $FeCl_3$, $FeSO_4{\cdot}7H_2O$, ferrozine, hydroxylamine hydrochloride, acetate buffer (pH 4.65) were Fluka p.a. reagents (Buchs, Switzerland) and used as received. Hydrogen peroxide (35%) was supplied by Merck AG (Darmstadt, Germany) and TiO_2 P25 (anastase to rutile ratio between 70:30 and 80:20) by Degussa. The Tedlar® A is a DuPont film (thickness: 72 μm) and consists of (–CH_2–CHF–) structural groups. The film is tough, flexible and heat resistant up to 180 °C (flowing point).

2.2. Photocatalyst preparation

Photoactive TiO_2 and/or iron oxide were deposited on commercial PVF films as polymeric substrate. Before use, the PVF films were washed in diethyl ether ethanol (1:1) mixture and in MilliQ water in order to eliminate surface contaminants. Three different preparation methods have been used:

(1) The first preparation method consisted in the application of a single TiO_2 photocatalytic surface functionalization-deposition (PSFD) treatment: The clean polymer substrates were attached around a cylindrical steel support and immersed in a photoreactor containing well dispersed suspensions of TiO_2 (0.2–1.7 g/L) at different pH (3, natural, 7, 11). The photoreactor was irradiated in a CPS Suntest system (ATLAS GmbH) during 2 h under magnetic stirring. Steel support was dimensioned to maintain the PVF film close to the surface of the photoreactor. This treatment leaded to the immobilization of TiO_2 particles on the functionalized PVF surface (PVF^f–TiO_2). The possible nature of polymer–TiO_2 bonding is proposed in Section 3.1.1.
(2) In the second preparation method, the iron oxide was immobilized on PVF substrates. Commercial PVF films were immersed in a 5 g/L solution of $FeCl_3$ and heated under stirring at 70, 80 or 90 °C during 1 h. Optionally, the composite material was heated in an oven at 100 °C for 1 h. The final film showed an iron oxide coat (PVF–Fe oxide).
(3) The third preparation method consisted in applying a TiO_2 PSFD treatment followed by iron oxide coating as described in method (1) and (2) to immobilize the TiO_2 and iron oxide on the PVF film leading to PVF^f–TiO_2–Fe oxide.

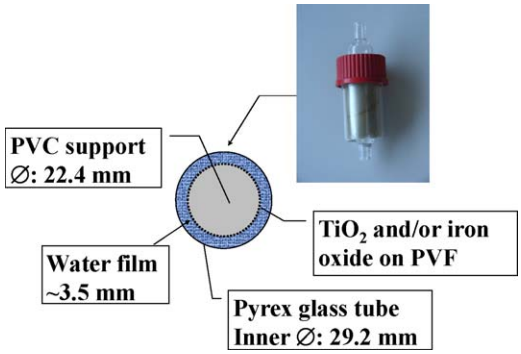

Fig. 1. Transversal cut and characteristics of the photo-reactor.

2.3. Photoreactor and irradiation procedure

All HQ degradation experiments were carried out under simulated solar light, using thin film Pyrex glass reactors (Fig. 1). A peristaltic pump allows circulation of water (flow rate of 100 mL/min) using an Erlenmeyer flask as a recirculation tank. The total volume of the system (110 mL) consists of two parts: 25 mL irradiated volume and the dead volume in connecting tubes and Erlenmeyer tank. Internal PVC supports were placed in the reactor to carry the photocatalyst films. The reactor was illuminated inside a solar simulator CPS Suntest system (Atlas GmbH). This solar box has a light spectral distribution with about 0.5% of the emitted photons below 300 nm, and 7% between 300 and 400 nm. The emission spectrum between 400 and 800 nm follows the solar spectrum. The irradiation experiments were started at room temperature (20 °C) and progressively the temperature increased up to approximately 30 °C. Three reactors were placed in parallel inside the solar box (Fig. 2). The degradation experiments were performed using solutions containing HQ (0.18 mM) and H_2O_2 (1.6 mM).

2.4. Analysis of the irradiated solutions

The quantitative determination of organic compounds was carried out by HPLC chromatography using a LC system HPLC-UV Shimadzu LC-2010A equipped with a UV detector. Samples, injected via an auto-sampler, were eluted at a flow rate of 1 mL/min through a column (Nucleosil C18 Marcherey Nagel) and using as mobile phase HPLC grade acetonitrile–acetic acid solution (10%) in a 40–60%. The total organic carbon (TOC) was monitored via an

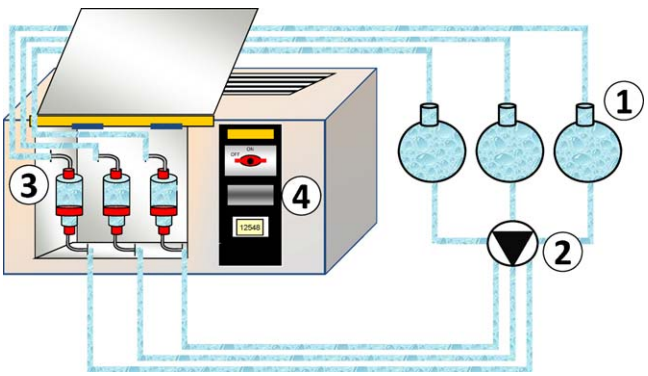

Fig. 2. Photocatalytic setup: (1) tanks, (2) peristaltic pump, (3) photo-reactors, and (4) solar simulator.

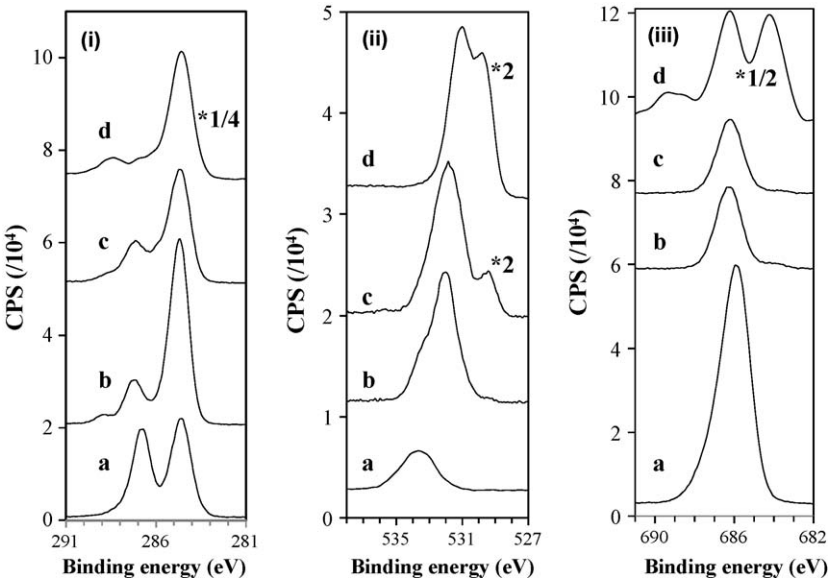

Fig. 3. X-ray photoelectron spectra of: (i) C (1s), (ii) O (1s), (iii) F (1s) core level photoelectron spectra of (a) PVF; (b) PVF after a TiO_2-PSFD treatment at pH 11; (c) PVF after a TiO_2 PSFD treatment at pH 3; and (d) PVF^f–TiO_2–Fe oxide (TiO_2 PSFD treatment at pH 3).

ASI automatic sample injector (Shimadzu 500). The peroxide concentrations were assessed by Merkoquant® paper at levels between 0.5 and 25 mg/L. The total iron concentration in the irradiated solutions was measured by complexation with Ferrozine® (Aldrich 16.060-1) in the presence of hydroxylamine hydrochloride and acetate buffer (pH 4.65) [30].

2.5. Photocatalyst characterization

2.5.1. X-ray photoelectron spectroscopy

X-ray photoelectron spectroscopy data were collected by Axis Ultra system (Kratos analytical, Manchester, UK) under ultra-high vacuum condition ($<10^{-8}$ Torr), using a monochromatic Al $K\alpha$ X-ray source (1486.6 eV) at the laboratory of Chemical Metallurgy at EPFL. The source power was maintained at 150 W (10 mA, 15 kV). The emitted photoelectrons were sampled from a square area of 750 μm × 350 μm. The gold (Au $4f_{7/2}$) and copper (Cu $2p_{3/2}$) lines at 84.0 and 932.6 eV respectively, were used for calibration, and the adventitious carbon 1s peak at 284.6 eV was used as an internal standard to compensate for charging effects.

2.5.2. SEM analysis

The surface morphology of the supports and the catalysts were investigated using a scanning electron microscope (Phillips XL30 SFEG) equipped with X-ray detector.

2.5.3. UV–vis spetrophotometry analysis

UV–vis spectra were recorded on a Varian Cary 5 equipped with an integration sphere.

3. Results and discussion

3.1. PVF^f–TiO_2–Fe oxide characterization

The XPS spectroscopy allows determining surface composition of the thin outermost surface layers. It also allows obtaining the elemental depth profile. XPS measurements were performed on PVF^f–TiO_2 and PVF^f–TiO_2–Fe oxide prepared under different pH condition. An energy shift to lower binding energies (BE) of about 3 eV was observed due to the low conductivity of the samples. In the present study, the corrected BEs are reported.

3.1.1. XPS study of the influence of pH on TiO_2 photocatalytic surface functionalization-deposition treatment of polyvinyl fluoride film

Different PVF^f–TiO_2 and PVF^f–TiO_2–Fe oxide samples have been produced by functionalization at various pHs. Fig. 3(i) presents the C (1s) carbon peaks at each preparation step. For the non-modified PVF film (trace a), there are two peaks: the higher peak centered at BE = 284.6 eV corresponding to $(CH_2)_n$ groups, the second centered at BE = 286.6 eV corresponding to C–F bond. The F/C atomic ratio for the PVF was 0.46, which is less than the theoretical stoichiometric value of 0.5 (Table 1). This slight difference can be attributed to hydrocarbon contamination and the presence of surface oxygen. After the TiO_2 PSFD treatment of PVF at pH 11, (trace b), the XPS spectrum changes with the appearance of C (1s) peaks at a BE of 287.2 and 289 eV corresponding to the formation of C═O bond of ketones and carboxylic acids respectively. This observation confirms that the TiO_2 PSFD treatment induces the formation of oxygen functional groups in agreement with a recent study by Kim et al. [31]. After TiO_2 PSFD treatment at pH 3 (trace c), the XPS spectrum was similar to the trace b excepting that the carboxylic acid peak at 289 eV is not visible and that the ratio C–H/C═O is considerably lower indicating a larger formation of oxygen-based groups at the Tedlar® surface at acidic pH.

Fig. 3(ii) shows the evolution of PVF surface oxygen peak O (1s) for different preparation steps. In trace a, the O (1s) peak is centered at BE = 533.7 eV corresponding to the oxygen contained in hydrocarbon contamination on the polymeric surface. After a TiO_2 PSFD treatment at pH 11, (trace b) the O (1s) peak is shifted to 532 eV, corresponding to the formation of C═O and COOH groups on the PVF surface. Trace (b) shows as well a small peak at 529.4 eV which corresponds to the oxygen in TiO_2 suggesting the presence of traces of this oxide on PVF surface. After a TiO_2 PSFD treatment at pH 3 (trace c), a significant O (1s) peak appears at BE = 529.4 eV

Table 1
Atomic composition of original polymer surface (PVF), TiO_2 PSFD treated polymer (PVF^f–TiO_2) at pH 3 and 11 (only principal constituents).

Samples	C	O	F	Ti	F/C	O/C
PVF	66.0	3.7	30.3	0	0.46	0.06
PVF^f–TiO_2 pH 11	80.4	10.3	9.3	0	0.11	0.12
PVF^f–TiO_2 pH 3	72.6	16.9	9.3	1.2	0.13	0.24

corresponding to the oxygen of the TiO_2 while the next peak at BE = 531.8 eV corresponds to O (1s) in C═O, COOH groups.

Fig. 3(iii) shows the changes in the F (1s) XPS spectrum due to TiO_2 PSFD treatment. For the non-modified PVF, the F (1s) signal consist of a single peak located at a BE of 685.9 eV. The main differences between non-modified PVF (trace a) and TiO_2 PSFD treated polymers (traces b and c) are a shift (of 0.3 eV) of F (1s) BE to the higher energy possibly due to the changes in the fluorine chemical environment and a decrease of the peak due to fluorine substitution.

Table 1 shows the atomic composition of PVF surface before and after TiO_2 PSFD treatment. From a semi-quantitative comparison of relative atomic percentage of oxygen, carbon, fluorine and titanium on the surface before and after TiO_2 PSFD treatment, it was found that this treatment led to an important increase in relative oxygen and carbon surface concentration and a concomitant decrease in the fluorine concentration. In Table 1 can be seen that the pH during TiO_2 PSFD treatment influences the surface modification. The surface O/C ratio changes from 0.06 in the non-modified PVF to 0.24 after a TiO_2 PSFD treatment at pH 3 and to 0.12 at pH 11. The surface F/C ratio changed from 0.46 in the non-modified PVF to 0.13 and 0.11 after a TiO_2 PSFD treatment at pH 3 and 11 respectively. Thus photocatalytic oxidation of the polymer surface induces the formation of oxygenic functional groups along the elimination of bounded fluorine.

Simultaneously, when submitting PVF to a TiO_2 PSFD treatment, the immobilization of the TiO_2 assisted by polymer surface functionalization occurs. Fig. 4 (traces a and b), shows the Ti (2p) core level photoelectron spectra characteristic of Ti in TiO_2 [32] after TiO_2 PSFD treatment at pH 3 and 11. Thus after the treatment performed at pH 3, the polymer is partially covered with TiO_2 (1.3% atomic percentage of the surface) whereas after treatment at pH 11, Titanium was not detected. These results show that it is possible to control the extent of TiO_2 deposition by varying the pH.

The simultaneous photocatalytic functionalization of PVF surface and a deposition of TiO_2 is illustrated in Fig. 5. As a matter of fact, under irradiation in aqueous TiO_2 suspension in equilibrium with air, PVF film suffers photocatalytic attacks leading to C═O, COOH groups and to the elimination of fluorine. When the pH of the aqueous solution is acidic, (i) the polymer surface is negatively charged since the TiO_2 PSFD treatment induced the formation of functional groups

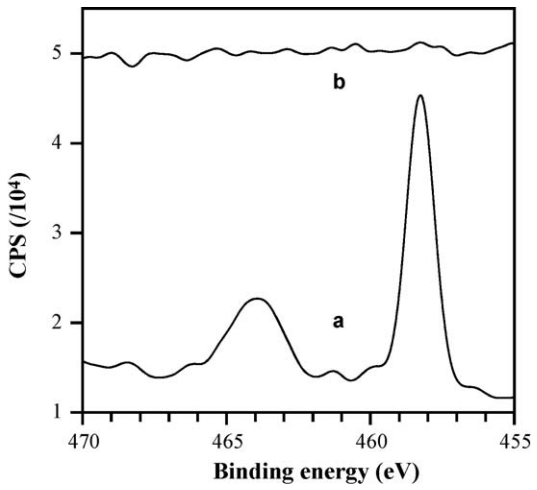

Fig. 4. X-ray photoelectron spectra of Ti (2p) in (a) PVF after a TiO_2 PSFD treatment at pH 3 and (b) PVF after a TiO_2 PSFD treatment at pH 11.

like COO^- and (ii) the superficial charge of TiO_2 P25 is positive since its isoelectric point is near to 7. Consequently an electrostatic attraction binds the TiO_2 particles to the polymer surface.

3.1.2. XPS studies of iron species and overall atomic profile of the PVF^f–TiO_2–Fe oxide photocatalyst

The deposition of iron oxide on PVF^f–TiO_2 surfaces was described under Section 2.2. The determination of chemical nature of the iron coating was investigated by XPS.

In Fig. 6, the iron peak was located at a BE of 711 eV which is characteristic of Fe^{3+} ions in akaganeite [33]. Nevertheless, the XPS results are not sufficient to determine with accuracy the nature of iron oxide present at polymer surface. However, various reports confirm this hypothesis, as the thermal hydrolysis of $FeCl_3$ solutions leads mainly to the formation of akaganeite [34].

In Fig. 3(iii), the XPS spectrum of F (1s) core level is presented. The PVF^f–TiO_2–Fe oxide spectrum (trace d), includes the triplet F (1s) peak with two predominant components at a BE of 684.2 and 686.3 eV. These two peaks correspond respectively to fluorine incorporated into iron oxide (FeOF) due to the anion exchange

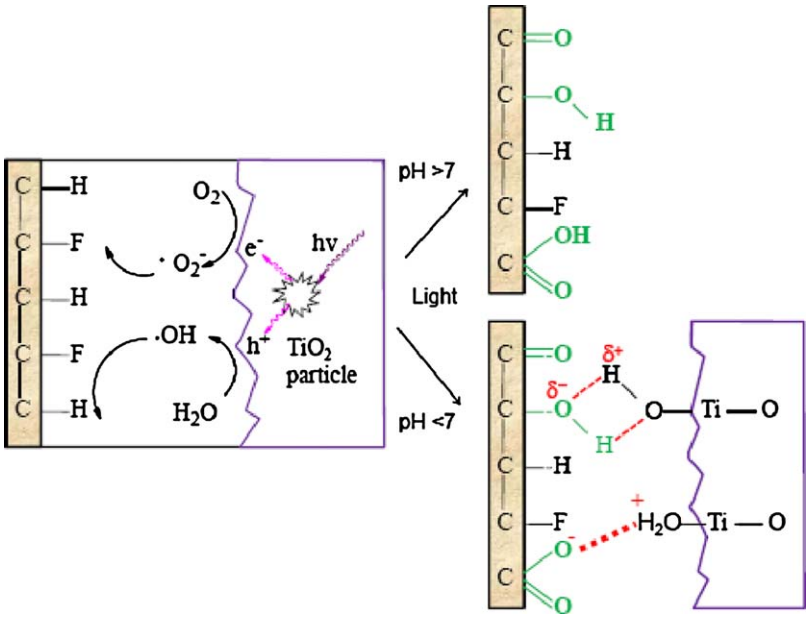

Fig. 5. Mechanistic proposition for TiO_2 photocatalytic surface functionalization-deposition as a function of pH.

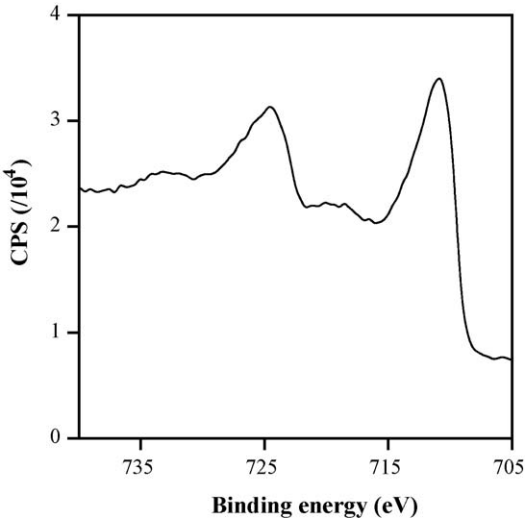

Fig. 6. Fe (2p) core level photoelectron spectra of PVF^f–TiO_2–Fe oxide.

properties of akaganeite [35], and to the polymeric C–F bond. The smaller F (1s) peak is centered at a BE = 689 eV corresponding to F^- ions adsorbed on the iron oxide surface.

Fig. 7 shows the XPS depth profile of PVF^f–TiO_2–Fe oxide surface indicating the atomic composition as a function of depth. Each minute, the topmost layer of about 2 nm depth was eroded by the Ar^+-ions sputtering. The reported values are approximations, since preferential sputtering effects cannot be excluded because the sputter rate for each investigated element is different and depends on its particular sensitivity factor. Fig. 7 shows the contamination of the first layer (about 5 nm) with hydrocarbons and oxygen. In the next layer of about 15 nm, iron, oxygen, fluorine and chlorine atomic concentration were seen to be close to their maximum value (35%, 35%, 18%, and 6% respectively) decreasing continuously with increasing depth. The atomic concentration of carbon follows an opposite tendency i.e. has its minimum value (10%) between 5 and 20 nm and then increases. Atomic concentration of Ti is zero until ~35 nm and then increases to reach a maximum value of 2.5% at ~100 nm. This result indicates that TiO_2 particles are located close enough to the surface of the catalyst to play a role in the degradation processes particularly if the photocatalyst has been reused several times and the iron oxide coat has been partially dissolved allowing the TiO_2 to diffuse to the surface. An XPS study of PVF^f–TiO_2–Fe oxide surface changes after reuse will be presented in another paper (part 2 of this work).

3.1.3. Scanning electron microscopy

Fig. 8 shows the SEM micrograph of polymer surface before and after the sequential TiO_2 PSFD and iron oxide coating.

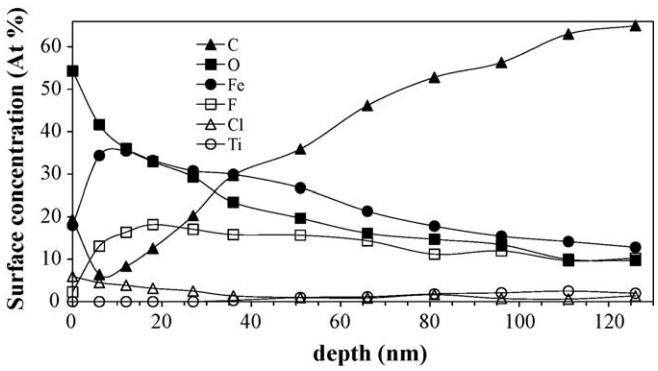

Fig. 7. Depth profile of PVF^f–TiO_2–Fe oxide (PSFD treatment at pH 3).

The non-modified PVF surface, Fig. 8a, is predominantly smooth. After a TiO_2 PSFD treatment at pH 5, aggregated TiO_2 particles cover a significant part of the surface exposed to the light irradiation (Fig. 8b) and to a lesser degree in the back side (Fig. 8c). This TiO_2 coating seems to increase the surface roughness favoring subsequent iron oxide nucleation around the TiO_2 particles. TiO_2 decrease the interfacial energy which is a limiting factor for the crystallization of iron oxide [36]. Fig. 8d shows the PVF^f–TiO_2–Fe oxide catalyst surface loaded with iron oxide aggregates of about 1 μm. These aggregates are composed of nanoparticles of approximately 50 nm, which seem to cover the polymer surface (Fig. 8e).

3.1.4. UV–vis absorbance study

Fig. 9 presents the UV–vis absorption of PVF^f–TiO_2, PVF–Fe oxide and PVF^f–TiO_2–Fe oxide composites between 350 and 700 nm. The absorbance of PVF in this region was negligible. For The PVF^f–TiO_2 (trace a) the UV–vis spectrum shows that this material only absorbs light below 400 nm, characteristic for TiO_2 particles. In contrast, PVF–Fe oxide (trace b) absorbs visible light. Its spectrum shows an important absorption for low wavelength (violet and UV light) and a shoulder between 550 and 450 nm (green–blue light). PVF^f–TiO_2–Fe oxide spectrum (trace c) presented a similar spectrum shape to trace b) but the observed absorption was 2 times higher. Thus, the PVF^f–TiO_2–Fe oxide UV–vis spectrum does not correspond to the sum of PVF^f–TiO_2 and PVF–Fe oxide spectra, which is due to a more significant iron oxide presence on the rough PVF^f–TiO_2 surface than on smooth PVF.

3.2. Photocatalytic activity

Fig. 10 presents the evolution of HQ within 240 min under different conditions. During photolysis and dark runs (both represented by trace a), HQ concentration remained constant: (i) HQ was resistant to direct photolysis by simulated solar light and (ii) no adsorption of HQ on PVF^f–TiO_2–Fe oxide was detectable. For photo-assisted reaction on PVF^f–TiO_2 (trace b) and on PVF^f–TiO_2–Fe oxide (trace c), 7% and 15% of HQ was degraded in 240 min of treatment. HQ degradation by the system PVF^f–TiO_2/H_2O_2/light (trace d) reached almost 40% whereas the system PVF^f–TiO_2–Fe oxide/H_2O_2 under dark (trace e) reached 50% of HQ degradation in 240 min by heterogeneous Fenton-like oxidation. For the system PVF–Fe oxide/H_2O_2/light (trace f), the HQ degradation rate remained low during an activation period of 30 min, but increased between 30 and 120 min of treatment with 10% and 97% degradation efficiency. This behavior is typical for iron photo-leaching during the first step of the reaction leading to a subsequent important contribution of the homogeneous process to HQ degradation after the first 60 min of treatment since 0.5 mg/L of dissolved iron ions have been detected by the ferrozine method. For heterogeneous reaction with the system PVF^f–TiO_2–Fe oxide/H_2O_2/light (trace g), HQ decreased very fast (91%) and with a constant slope typical of heterogeneous processes during the first 60 min. Only 0.2 mg/L of dissolved iron ions were detected at the end of this process. Consequently, the influence of homogeneous photo-Fenton processes on HQ degradation is small. A more accurate estimation of homogeneous contribution will be proposed in another paper (part 2 of this work).

The evolution of the TOC versus time for some processes is illustrated in Fig. 11. For the system PVF^f–TiO_2–Fe oxide/H_2O_2, under dark, no mineralization was observed (trace a). Homogeneous photo-Fenton process (Fe^{2+} (0.3 mg/L)/H_2O_2/light) mineralized about 60% of TOC after 240 min (trace b). Using PVF–Fe oxide/H_2O_2/light system (trace c), the TOC increased during the first 30 min, due to a degradation of the polymer substrate by

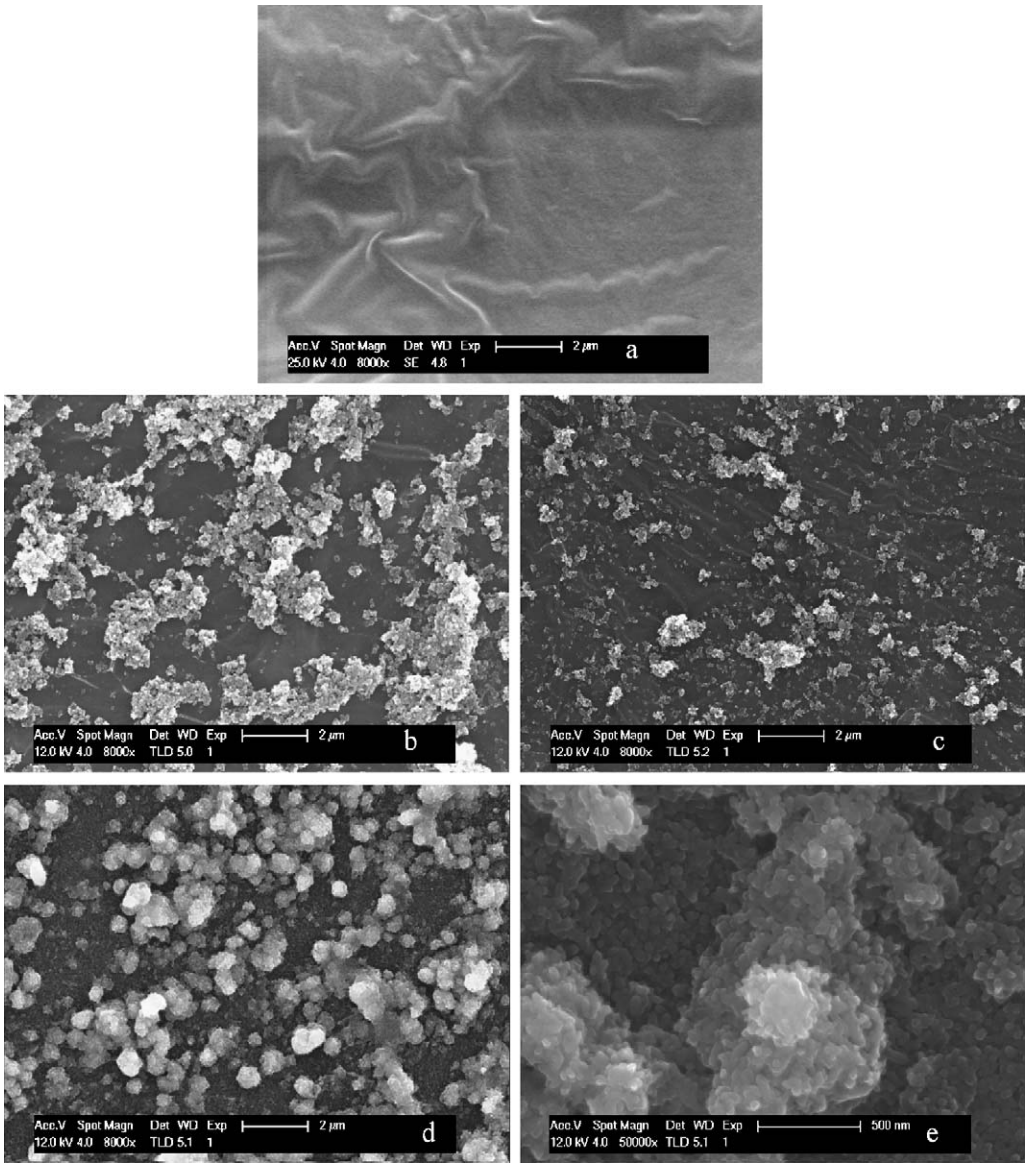

Fig. 8. Scanning electron microscopic images of: (a) PVF, (b) PVF^f–TiO_2 prepared at pH 5 (external side), (c) PVF^f–TiO_2 prepared at pH 5 (internal side), and (d)–(e) PVF^f–TiO_2–Fe oxide prepared at pH 5.

generated radicals. Thereafter, the TOC concentration decreased rapidly up to 80% within 240 min (essentially due to mineralization caused by dissolved iron ions). TOC removal by the system PVF^f–TiO_2–Fe oxide/H_2O_2/light (trace d) was the fastest achieving a mineralization of 95% after 240 min. For each process, the residual H_2O_2 concentrations were measured; in no case the initially added H_2O_2 was totally consumed. The decrease of mineralization rates between 180 and 240 min (traces c and d) is therefore limited by diffusion.

During the photo-assisted reaction on PVF^f–TiO_2–Fe oxide in presence of H_2O_2, besides Eqs. (2) and (3), the ≡Fe(II) regeneration (which is the rate determinant step of Fenton reaction) could occur via the photo-reduction of ≡Fe(III) species including hydroxy- or organo-complexes (Eqs. (5) and (6)). Additionally photo-induced reactive species (electron–hole pair) are probably formed on iron oxide under illumination enhancing HQ degradation rates (Eq. (7)). Conduction band electrons could react with H_2O_2 to form hydroxyl radicals (Eq. (8)) or could participate in the regeneration of ≡Fe(II) species (Eq. (9)). Valence band holes may oxidize the pollutant (Eq. (10)) [17] (≡Fe(II) and ≡Fe(III) represent the Fe(II)/Fe(III) species in solid or solution phase).

$$\equiv Fe(II) + H_2O_2 \rightarrow \equiv Fe(III) + OH^{\bullet} + OH^{-} \quad (k \approx 40\text{–}80\ M/s) \tag{1}$$

$$\equiv Fe(III) + H_2O_2 \rightarrow \equiv Fe(II) + HO_2^{\bullet} + H^{+} \quad (k \approx 0.003\ M/s) \tag{2}$$

$$\equiv Fe(III) + O_2^{-\bullet} \rightarrow \equiv Fe(II) + O_2 \tag{3}$$

$$\equiv Fe(II) + O_2^{-\bullet} \rightarrow \equiv Fe(III) + O_2^{2-} \tag{4}$$

$$\equiv Fe(III)(OH)^{2+} + h\nu \rightarrow \equiv Fe(II) + OH^{\bullet} \tag{5}$$

$$\equiv Fe(III)L_n + h\nu \rightarrow \equiv Fe(II)L_{n-1} + L_{ox}^{+\bullet} \tag{6}$$

$$\text{Fe oxide} + h\nu \rightarrow \text{Fe oxide}(e^- + h^+) \tag{7}$$

$$\text{Fe oxide}(e^-) + H_2O_2 \rightarrow \text{Fe oxide} + OH^{\bullet} + OH^- \tag{8}$$

$$\text{Fe oxide}(e^-) + \equiv\text{Fe(III)} \rightarrow \text{Fe oxide} + \equiv\text{Fe(II)} \quad (9)$$

$$\text{Fe oxide}(h^+) + R_{ad} \rightarrow \text{Fe oxide} + R_{ad}{}^{+\bullet} \quad (10)$$

Beside photo-Fenton oxidation (Eqs. (1)–(6)) and iron oxide photocatalysis (Eqs. (7)–(10)), other reactions may occur mediated by PVF^f–TiO_2–Fe oxide/H_2O_2/light involving electron–hole pair formation by TiO_2 band-gap illumination ($\lambda < 400$ nm). These reactions lead to radicals active in the degradation process as described in Eqs. (11)–(16).

$$TiO_2 + h\nu \rightarrow TiO_2(e^- + h^+) \quad (11)$$

$$TiO_2(h^+) + R_{ad} \rightarrow TiO_2 + R_{ad}{}^{+\bullet} \quad (12)$$

$$TiO_2(h^+) + H_2O \rightarrow TiO_2 + OH^\bullet + H^+ \quad (13)$$

$$TiO_2(e^-) + R_{ad} \rightarrow TiO_2 + R_{ad}{}^{-\bullet} \quad (14)$$

$$TiO_2(e^-) + O_2 \rightarrow TiO_2 + O_2{}^{-\bullet} \quad (15)$$

$$TiO_2(e^-) + H_2O_2 \rightarrow TiO_2 + OH^\bullet + OH^- \quad (16)$$

Furthermore, synergistic effects are likely to occur between TiO_2, iron oxide, dissolved iron ions, and functionalized polymer surface, accelerating HQ degradation in the presence of H_2O_2 as the electron acceptor.

3.3. Synergistic effects

Synergistic effects can be quantified by the synergistic factor S defined in Eq. (17), where R_0 represents the initial rate of degradation for a given process (Eq. (18)).

$$S = \frac{R_0(AB)}{R_0(A) + R_0(B)} \quad (17)$$

$$R_0 = \frac{[HQ]_0 - [HQ]_{30}}{30} \quad (18)$$

In the system PVF^f–TiO_2–Fe oxide/H_2O_2/light, the overall process is a combination of polymer supported TiO_2 and iron oxide photocatalysis associated with heterogeneous and homogeneous photo-Fenton oxidation. The exact assessment of synergistic effects in this system is not easy due to the difficulty to prepare PVF–Fe oxide and PVF^f–TiO_2–Fe oxide samples with the same iron oxide load. An approximated synergistic factor can be estimated assuming that (1) The photocatalyst UV–vis extinction coefficients between 450 and 550 nm (Fig. 9) are proportional to the amount of iron oxide present on the PVF surface and (2) the photocatalytic activity of PVF–Fe oxide increases linearly with the amount of immobilized iron oxide.

The initial HQ degradation rates (R_0) have been calculated during the first 30 min for different photo-assisted processes (Eq. (18)) from the decay curves b, d, e, f, and g in Fig. 10 and are represented in Table 2.

These rates are representative for the heterogeneous reactions since at the beginning of the process, a low amount of iron is dissolved (<0.1 mg/L). The rate R_0 corresponding to a virtual PVF–Fe oxide containing the same amount of iron oxide as a PVF^f–TiO_2–Fe oxide was estimated according to assumptions (1) and (2). A correction factor C, defined in Eq. (19) as the integrated absorbance of PVF^f–TiO_2–Fe oxide (trace c) over the integrated absorbance of PVF–Fe oxide (trace b) from 450 to 550 nm (where the TiO_2 absorbance is insignificant), was calculated from Fig. 9.

$$C = \int_{450}^{550} \left[\frac{A(\text{PVF}^f - TiO_2 - \text{Fe oxide})}{A(\text{PVF} - \text{Fe oxide})} \right] = 2.2 \quad (19)$$

Table 2
Initial HQ degradation rates relative to different photo-assisted processes.

Photo-process	R_0 (μmol/min)
H_2O_2	0.14
PVF^f–TiO_2	0.08
(PVF^f–TiO_2)/H_2O_2	0.29[a]
(PVF–Fe oxide)/H_2O_2	0.57[b]
(PVF–Fe oxide)$_{virtual}$[c]/H_2O_2	1.3[d]
(PVF^f–TiO_2–Fe oxide)/H_2O_2	4.0[e]

[a] Value calculated from decay curve d of Fig. 10.
[b] Value calculated from decay curve f of Fig. 10.
[c] Virtual photocatalyst containing the same amount of iron oxide as PVF^f–TiO_2–Fe oxide.
[d] Rate estimated from footnote (a) and from Eqs. (19) and (20) and Fig. 9.
[e] Value calculated from decay curve g of Fig. 10.

Multiplying R_0(PVF–Fe oxide/H_2O_2/light) by C we can estimate R_0(PVF–Fe oxide/H_2O_2/light)$_{virtual}$ corresponding to the degradation rate relative to a PVF–Fe oxide with an iron oxide load as PVF^f–TiO_2–Fe oxide (Eq. (20)):

$$R_0(\text{PVF} - \text{Fe oxide}/H_2O_2/\text{light})_{virtual} = C * R_0(\text{PVF} - \text{Fe oxide}/H_2O_2/\text{light}) \quad (20)$$

Replacing $R_0(A)$, $R_0(B)$ and $R_0(AB)$ in Eq. (17) by the values of R_0(PVF^f–TiO_2/H_2O_2/light), R_0(PVF–Fe oxide/H_2O_2/light)$_{virtual}$ and R_0(PVF^f–TiO_2–Fe oxide/H_2O_2/light) (from Table 2) respectively, the synergistic factor S can be calculated. A value of $S \approx 2.5$ was obtained, meaning that the rate relative to the combined processes is 2.5 times faster than the sum of rates relative to the separated processes. Compared to previous studies [25–27], this result suggests the presence of a significant synergistic effect in the system PVF^f–TiO_2–Fe oxide/H_2O_2/light.

At the beginning of the treatment (for which S factor has been calculated), the combination of homogeneous photo-Fenton and TiO_2 photocatalysis is probably not the essential interaction. Indeed the concentration of dissolved iron ions is low (about 0.1 mg/L) as well as the relative atomic surface concentration of titanium (0.3%) obtained by XPS after utilization of PVF^f–TiO_2–Fe oxide. A more plausible suggestion would be that heterogeneous interactions between supported iron oxide and TiO_2 under irradiation are responsible of significant part of the observed

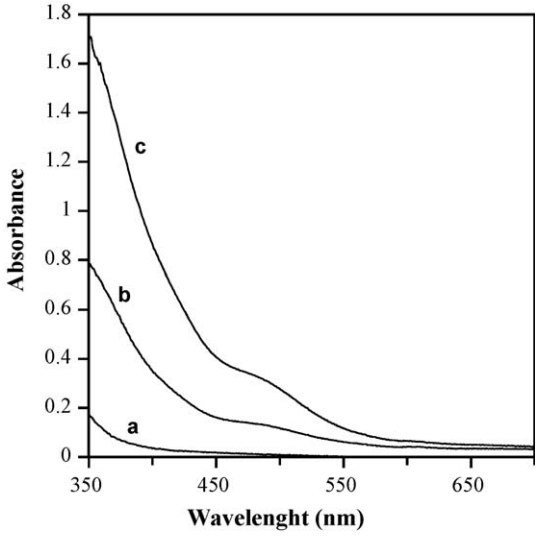

Fig. 9. UV–vis absorption spectrum of: (a) PVF^f–TiO_2, (b) PVF–Fe oxide, (c) PVF^f–TiO_2–Fe oxide.

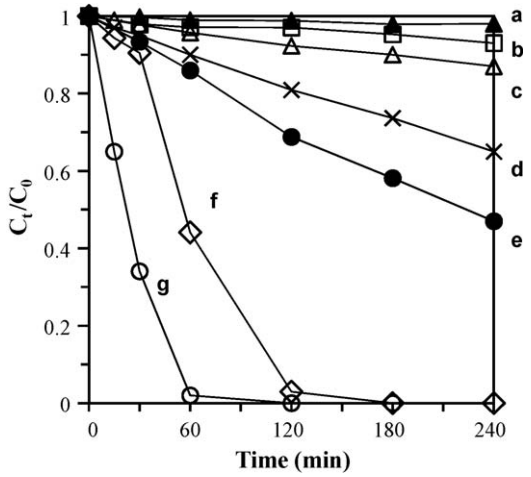

Fig. 10. Degradation of 0.18 mM of HQ, initial pH 5.7, 75 cm^2 of heterogeneous photocatalyst 1.6 mM H_2O_2 under solar simulation: (a) bare light/dark adsorption, (b) PVF–TiO_2/light, (c) PVF^f–TiO_2–Fe oxide/light, (d) PVF^f–TiO_2/H_2O_2/light, (e) PVF^f–TiO_2–Fe oxide/H_2O_2, (f) PVF–Fe oxide/H_2O_2/light, and (g) PVF^f–TiO_2–Fe oxide/H_2O_2/light. The traces represent an average of three consecutive runs using the same photocatalysts (first run not included).

synergistic effects. This interaction has been investigated recently by double-beam photoacoustic spectroscopy [37] and was suggested to depend on the irradiation wavelength:

(i) Under ultraviolet irradiation, photoexcited electrons generated in TiO_2 catalyst (Eq. (11)) could be trapped into iron oxide particles (Eq. (21)) resulting in improvement of charge separation on TiO_2 (completed by an oxidation reaction performed by remaining hole Eq. (12) and (13)), and, in regeneration of ≡Fe(II) sites (Eq. (9)) (accelerating photo-Fenton reaction rates) by reduction of Fe(III) species.

$$\text{Fe oxide} + TiO_2(e^-) \rightarrow \text{Fe oxide}(e^-) + TiO_2 \quad (21)$$

This electron transfer is possible since the electrochemical potential position of TiO_2 bands relative to those of iron oxides [38] allows electron transfer from excited TiO_2 valence band to iron oxide valence band by formation of a heterojunction. This mechanism is represented in Fig. 12(a).

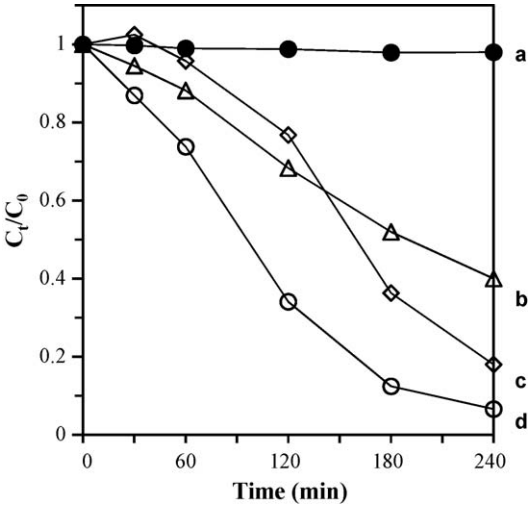

Fig. 11. TOC removal of 0.18 mM of HQ, initial pH 5.7, 75 cm^2 of heterogeneous photocatalyst 1.6 mM H_2O_2 under solar simulation: (a) PVF^f–TiO_2–Fe oxide/H_2O_2, (b) Fe^{2+} (0.3 mg/L)/H_2O_2/light, (c) PVF–Fe oxide/H_2O_2/light, and (d) PVF^f–TiO_2–Fe oxide/H_2O_2/light. The traces represent an average of three consecutive runs using the same photocatalysts (first run not included).

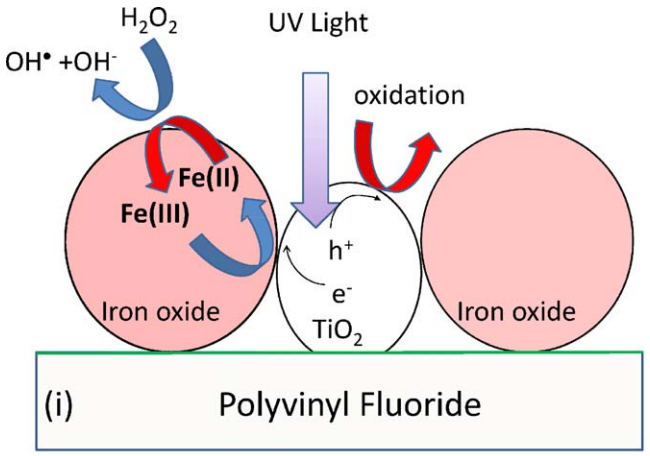

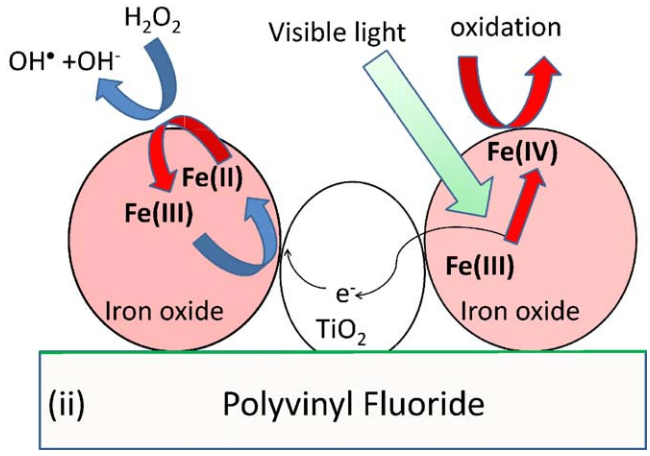

Fig. 12. Schematic representation of possible synergistic photocatalytic action in the system PVF^f–TiO_2–Fe oxide/H_2O_2/light: (i) under visible light irradiation and (ii) under ultraviolet light irradiation.

(ii) Under visible light irradiation, iron oxide (or complex) could act as a sensitizer for TiO_2. First, a photo-excited iron species would inject an electron into TiO_2 and become oxidized. Then, the oxidized iron species (Fe(IV)) oxidize hydroquinone (polymer surface or ligand) to go back to their initial state (Fe(III)), whereas the electron injected in TiO_2 is transferred to iron oxide regenerating Fe(II). This mechanism which is described in Fig. 12 (b) needs further confirmation and solid evidence, due to the involvement of Fe(IV) oxidized species.

3.4. Effect of PVF^f–TiO_2–Fe oxide preparation parameters on HQ degradation rates

3.4.1. Effect of the pH during TiO_2 PSFD treatment on HQ degradation rates for the system PVF^f–TiO_2–Fe oxide/H_2O_2/light

The initial pH of the aqueous media during the TiO_2 PSFD treatment determines the amount of oxygenated groups formed and the superficial charge of TiO_2 nanoparticles. The extent of TiO_2 photo-deposition depends on pH as well (Table 1). At acidic pH, the TiO_2 being positively charged can be stably deposited on electronegative oxygenated groups on the polymer surface. At basic pH, the TiO_2 and polymer are both negatively charged and the interaction is repulsive, limiting the polymer functionalization and the TiO_2 deposition. Consequently, since iron oxide crystallization is favored by TiO_2 presence, less iron oxide is deposited on its surface leading to a less efficient PVF^f–TiO_2–Fe oxide photocatalyst. HQ mineralization rates by PVF^f–TiO_2–Fe oxide/H_2O_2/light decrease as the pH for TiO_2 PSFD treatment increased with 72%,

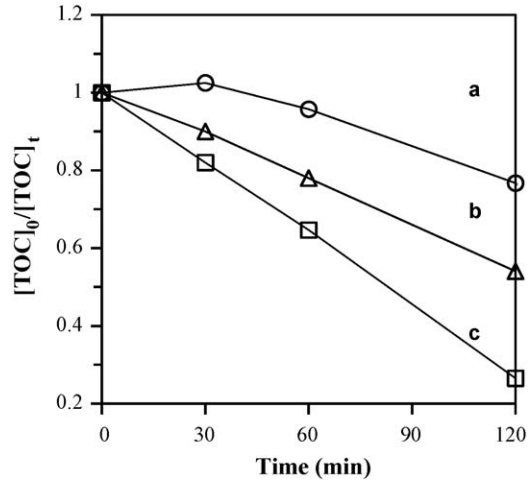

Fig. 13. TOC removal of 0.18 mM of HQ, initial pH 5.7, 75 cm^2 of heterogeneous photocatalyst 1.6 mM H_2O_2 under solar simulation: (a) PVF–Fe oxide/H_2O_2/light, (b) PVF^f–TiO_2–Fe oxide (PSFD treatment at pH 11)/H_2O_2/light, and (c) PVF^f–TiO_2–Fe oxide (PSFD treatment at pH 3)/H_2O_2/light.

68% and 46% of HQ mineralized after 120 min for pH 3, 7 and 11 respectively. Fig. 13 represents TOC removal by different photocatalyst during HQ degradation in presence of H_2O_2 under light. The disparity between PVF–Fe oxide (trace a), and PVF^f–TiO_2–Fe oxide prepared at pH 11 and 3 (traces b and c) shows the advantage of applying the TiO_2 PSFD treatment before iron oxide coating. Indeed at pH 3, more TiO_2 fixation induces as well more iron oxide coating. The TiO_2 PSFD treatment also avoids the initial TOC increase by the PVF–Fe oxide /H_2O_2/light system as the polymer already was degraded to a stable state under this treatment. In general, TOC removal is faster for the TiO_2 PSFD treated polymers particularly when the PSFD was carried out at acidic pHs.

3.4.2. Effect of TiO_2 concentration used for the TiO_2 PSFD treatment on HQ mineralization by the system PVF^f–TiO_2–Fe oxide/H_2O_2/light

Fig. 14 shows that maximum HQ mineralization under light is reached when TiO_2 concentration used during PSFD treatment is ~1 g/L. The TiO_2 concentration influences both the extent of polymer surface functionalization and the amount of deposited TiO_2. Fig. 14 shows that during PSFD treatment, the first run (curve a) of photocatalytic mineralization is less efficient than following one (curve b). Thus, the first photocatalytic run enhances the photocatalyst performance for subsequent runs.

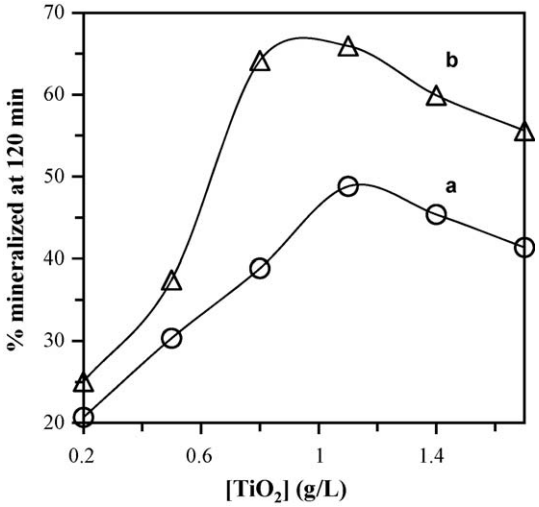

Fig. 14. Effect of TiO_2 concentration (used for previous PSFD treatment of PVF) on HQ mineralization (of 0.18 mM HQ, initial pH 5.7, PVF^f–TiO_2–Fe oxide 75 cm^2, H_2O_2 1.6 mM under solar simulation): (a) first and (b) second consecutive HQ degradation.

3.4.3. Effect of iron oxide coating conditions on HQ mineralization by the system PVF^f–TiO_2–Fe oxide/H_2O_2/light

$FeCl_3$ hydrolysis was carried out at different temperatures (70, 80 and 90 °C) for the iron oxide generation and deposition. Applied temperatures during hydrolysis were found to play a significant role only for mineralization efficiency during the first degradation run: as temperature during hydrolysis was increased the mineralization rate during first run increased. During the following runs, HQ mineralization was similar for photocatalysts prepared at 70, 80 or 90 °C. This may be due to the formation of oxide during the hydrolysis at low temperatures, which is stabilized during the first run. This adaptation phase as well as PVF^f–TiO_2–Fe oxide long-term stability will be discussed separately in part 2 of this work.

An additional thermal treatment at 100 °C during 1 h after hydrolysis was applied to PVF^f–TiO_2–Fe oxide. The results obtained concerning HQ degradation have shown that this additional treatment was useless. Actually a temperature of 100 °C is not sufficiently high to induce phase changes of iron oxide or to melt PVF substrate.

4. Conclusions

- This work presents an innovative and simple way to prepare a highly photoactive catalyst combining TiO_2 and iron oxide fixed on PVF films.
- The surface characterization of photocatalyst shows that the PSFD treatment induced simultaneous surface functionalization involving oxygen-surface species formation and deposition of TiO_2 on carboxylic groups due to an electrostatic attraction.
- The TiO_2 deposition occurred preferentially when pH $\leq$ 7 and the activity of photocatalysts increased with acidity during PSFD treatment.
- The TiO_2 and iron oxide on PVF was an efficient material toward HQ degradation and mineralization under light in the presence of H_2O_2, at ambient temperature and neutral pH.
- Synergistic effects between TiO_2 and iron oxide for the system PVF^f–TiO_2–Fe oxide/H_2O_2/light were found to be significant and a synergistic factor *S* around 2.5 was estimated. These synergistic effects were assigned to the regeneration of ≡Fe(II) which is the rate-limiting step in Fenton processes.

Acknowledgements

F. Mazille wishes to express his gratitude to Pierre-Yves Pfirter, Nicolas Xanthopoulos and Robin Humphry-Baker for SEM, XPS, and UV–vis measurements respectively, to Dorothea Spuhler and John Kiwi for reviewing of phrasing. The authors wish to thank the European Commission for its financial support under the INNOWATECH project (contract no. 036882) within the thematic priority Global Change and Ecosystems of the Sixth Framework Program (FP6-2005-Global 4-SUSTDEV-2005-3.II.3.2).

References

[1] C. Pulgarin, J. Kiwi, Chimia 50 (1996) 50–55.
[2] D.S. Bhatkhande, V.G. Pangarkar, A.A.C.M. Beenackers, J. Chem. Technol. Biotechnol. 77 (2001) 102–116.
[3] K. Demeestere, J. Dewulf, H. Van Langenhove, Crit. Rev. Environ. Sci. Technol. 37 (2007) 489–538.
[4] A.-G. Rincón, C. Pulgarin, Catal. Today 124 (2007) 204–214.
[5] G. Palmisano, V. Augugliaro, M. Pagliaro, L. Palmisano, Chem. Commun. 33 (2007) 3425–3437.

[6] I. Munoz, J. Rieradevall, F. Torrades, J. Peral, X. Domènech, Sol. Energy 79 (2005) 369–375.
[7] J.J. Pignatello, E. Oliveros, A. MacKay, Crit. Rev. Environ. Sci. Technol. 36 (2006) 1–84.
[8] S. Parra, S. Malato, C. Pulgarin, Appl. Catal. B 36 (2002) 131–144.
[9] D. Gumy, A.G. Rincon, R. Hajdu, C. Pulgarin, Sol. Energy 80 (2006) 1376–1381.
[10] S.N. Hosseini, S.M. Borghei, M. Vossoughi, N. Taghavinia, Appl. Catal. B 74 (2007) 53–62.
[11] Y. Zhiyong, D. Laub, M. Bensimon, J. Kiwi, Inorg. Chim. Acta 361 (2008) 589–594.
[12] K.T. Ranjit, B. Viswanathan, J. Photochem. Photobiol. A: Chem. 108 (1997) 79–84.
[13] S. Sakthivel, H. Kisch, Angew. Chem. Int. 42 (2003) 4908–4911.
[14] J.A. Rengifo-Herrera, E. Mielczarski, J. Mielczarski, N.C. Castillo, J. Kiwi, C. Pulgarin, Appl. Catal. B 84 (2008) 448–456.
[15] J. Fernandez, J. Bandara, A. Lopez, Ph. Buffat, J. Kiwi, Langmuir 15 (1999) 185–192.
[16] D. Gumy, P. Fernandez-Ibanez, S. Malato, C. Pulgarin, O. Enea, J. Kiwi, Catal. Today 101 (2005) 375–382.
[17] J. Bandara, U. Klehm, J. Kiwi, Appl. Catal. B 76 (2007) 73–81.
[18] F. Martínez, G. Calleja, J.A. Melero, R. Molina, Appl. Catal. B 70 (2007) 452–460.
[19] J. Ramirez, C. Costa, L. Madeira, G. Mata, M. Vicente, M. Rojas-Cervantes, A. Lopez-Peinado, R. Martin-Aranda, Appl. Catal. B 71 (2007) 44–56.
[20] A. Moncayo, R.A. Torres-Palma, J. Kiwi, N. Benítez, C. Pulgarin, Appl. Catal. B 84 (2008) 577–583.
[21] M.R. Dhananjeyan, E. Mielczarski, K.R. Thampi, Ph. Buffat, M. Bensimon, A. Kulik, J. Mielczarski, J. Kiwi, J. Phys. Chem. B 105 (2001) 12046–12055.
[22] W.P. Kwan, B.M. Voelker, Environ. Sci. Technol. 36 (2002) 1467–1476.
[23] E. Celik, A.Y. Yildiz, N.F. Ak Azem, M. Tanoglu, M. Toparli, O.F. Emrullahoglu, I. Ozdemir, Mater. Sci. Eng. B 129 (2006) 193–199.
[24] X. Zhang, L. Lei, Appl. Surf. Sci. 254 (2008) 2406–2412.
[25] R.A. Torres, J.I. Nieto, E. Combet, C. Pétrier, C. Pulgarin, Appl. Catal. B 80 (2008) 165–175.
[26] L. Zou, B. Zhu, J. Photochem. Photobiol. A: Chem. 196 (2008) 24–32.
[27] P. Bouras, P. Lianos, Catal. Lett 123 (2008) 220–225.
[28] G.G. Kim, J.A. Kang, J.H. Kim, S.J. Kim, N.H. Lee, S.J. Kim, Surf. Coat. Technol. 201 (2006) 3761–3766.
[29] G.G. Kim, J.A. Kang, J.H. Kim, K.-Y. Lee, S.J. Kim, S.-J. Kim, Scripta Mater. 56 (2007) 349–351.
[30] E. Viollier, P.W. Inglett, K. Hunter, A.N. Roychoudhury, P. Van Cappellen, Appl. Geochem. 15 (2000) 785–790.
[31] G.G. Kim, J.A. Kang, S.J. Kim, S.H. Shin, S.J. Kim, J. Alloys Compd. 449 (2008) 184–187.
[32] J. Chastain, J.F. Moulder, Handbook of X-Ray Photoelectron Spectroscopy, Perkin Elmer Corporation, 1992, pp. 72–73.
[33] E.A. Deliyanni, L. Nalbandian, K.A. Matis, J. Colloid Interface Sci. 302 (2006) 458–466.
[34] S. Musić, S. Krehula, S. Popović, Z. Skoko, Mater. Lett. 57 (2003) 1096–1102.
[35] J. Cai, J. Liu, Z. Gao, A. Navrotsky, S.L. Suib, Chem. Mater. 13 (2001) 4595–4602.
[36] A.L. Greer, T.E. Quested, Philos. Mag. 86 (2006) 3665–3680.
[37] N. Murakami, T. Chiyoya, T. Tsubota, T. Ohno, Appl. Catal. A 348 (2008) 148–152.
[38] W. Zhang, Y. Chen, S. Yu, S. Chen, Y. Yin, Thin Solid Films 516 (2008) 4690–4694.